

# ShareTrace: Contact Tracing with Asynchronous, Parallel Message Passing on a Temporal Graph

**Ryan Tatton**

Case Western Reserve University, USA

RYAN.TATTON@CASE.EDU

**Erman Ayday**

Case Western Reserve University, USA

ERMAN.AYDAY@CASE.EDU

**Youngjin Yoo**

Case Western Reserve University, USA

YOUNGJIN.YOO@CASE.EDU

**Anisa Halimi\***

IBM Research Europe – Dublin, Ireland

ANISA.HALIMI@IBM.COM

## Abstract

Proximity-based contact tracing relies on user device interaction to estimate the spread of disease. ShareTrace is one such approach that has been shown to provide improved efficacy in tracking the spread of disease by also considering (in)direct forms of contact. In this work, we aim to provide an efficient and scalable formulation of ShareTrace by utilizing asynchronous, parallel, non-iterative message passing on a temporal graph. We also introduce a unique form of reachability, message reachability, that accounts for the dynamic nature of message passing and the temporal graph. Our evaluation on both synthetic and real-world temporal graphs indicates that correct parameter values optimize for accuracy and efficiency. In addition, we demonstrate that message reachability can accurately estimate the impact of the risk of a user on their contacts.

**Data and Code Availability** We utilize data sets that were collected through the SocioPatterns collaboration<sup>1</sup>. Specifically, we use face-to-face contact data in the setting of a high school [Thiers13] (Fournet and Barrat, 2014), a workplace [InVS15], and a scientific conference [SFHH] (G’enois and Barrat, 2018). These data sets are freely available to other researchers. The code associated with all algorithms and evaluation can be found on GitHub<sup>2</sup>.

\* This work was completed while the author was at Case Western Reserve University.

1. <http://www.sociopatterns.org>  
 2. <https://github.com/share-trace>

## 1. Introduction

ShareTrace is a privacy-preserving contact-tracing solution (Ayday et al., 2021). Unlike other approaches that rely on device proximity to detect human interaction, ShareTrace executes iterative message passing on a factor graph to estimate the marginal posterior probability of infection. To indicate its similarity to belief propagation, we shall herein refer to the ShareTrace algorithm as *risk propagation*. By considering both direct and indirect contact between users, Ayday et al. (2021) demonstrate that risk propagation is more effective than other proximity-based approaches that only consider direct forms of contact.

Building upon the efforts of Ayday et al. (2021), we provide an efficient and scalable formulation of risk propagation that utilizes asynchronous, parallel, non-iterative message passing on a temporal graph (Holme and Saramäki, 2012; Holme, 2015). While message passing has been studied under specific epidemiological models (Karrer and Newman, 2010; Li and Saad, 2021), our formulation allows us to contextualize risk propagation as a novel usage of a temporal graph that does not require such assumptions to infer the transmission of disease. As a result, we introduce a form of reachability that can uniquely characterize the dynamics of message passing on a temporal graph. Our formulation of risk propagation aligns with its distributed extension, as introduced by Ayday et al. (2021), which has connections to the actor model of concurrent computing (Baker and Hewitt, 1977; Agha, 1986) and the “think-like-a-vertex” model of graph processing algorithms (McCune et al., 2015).

Our in-depth explanation of risk propagation emphasizes the nuance of the algorithmic details and highlights important modifications to the original formulation by Ayday et al. (2021) that provide improved performance. Our evaluation aims (1) to describe the efficiency of risk propagation on both synthetic and real-world temporal graphs; (2) validate the accuracy of our new form of reachability on both synthetic and real-world graphs; (3) and briefly quantify the scalability of this implementation of risk propagation on synthetic graphs. To keep the scope of this work focused, we defer to Ayday et al. (2021) on the privacy and security aspects of ShareTrace.

## 2. Related Work

Since the beginning of the COVID-19 pandemic, there has been a copious amount of research in mobile contact tracing solutions, most notably being the joint effort by Apple and Google (2021). We do not attempt to provide an exhaustive reference to related work, but instead defer to external reviews and surveys that provide extensive comparison of existing solutions through the lenses of privacy, security, ethics, adversarial models, data management, scalability, interoperability, and more. Ahmed et al. (2020) and Martin et al. (2020) provide particularly thorough reviews of existing mobile contact tracing solutions with discussion of the techniques, privacy, security, and adversarial models. The former offers additional detail on the system architecture (i.e., centralized, decentralized, and hybrid), data management, and user concerns of existing solutions. Other notable reviews with similar discussion include Wen et al. (2020); Raskar et al. (2020); Cho et al. (2020); Dar et al. (2020); Lucivero et al. (2020). Kuhn et al. (2021) provides a formal framework for defining aspects of privacy in the context of proximity-based contact tracing.

## 3. Proposed Scheme

### 3.1. Preliminaries

We assume a system model in which each user owns a smart mobile device that has device-proximity detectability (e.g., Bluetooth). Furthermore, we assume that proximal interactions between user devices subsequently allow their devices, or a digital proxy thereof, to exchange messages over several days.

In risk propagation, the computation of infection risk is an inference problem in which the task is to estimate the marginal posterior probability of infection (MPPI). The prior probability of infection is derived from user symptoms (Menni et al., 2020). We shall refer to this probability, along with the time at which it is computed, as a *symptom score*. The posterior probability of infection also considers direct and indirect contact the user has with others. Thus, we shall call this probability an *exposure score*. In general, a *risk score*  $(r, t)$  is a timestamped probability of infection where  $r \in \mathbb{R}_{[0,1]}$  is the *magnitude* of the risk score and  $t \in \mathbb{R}_{\geq 0}$  is the *time* of its computation. We use  $r$  or  $t$  when only referring to one aspect of a risk score to avoid ambiguity.

Computing the full joint probability distribution is intractable as it scales exponentially in the number of users. To circumvent this challenge, risk propagation uses message passing on a factor graph to efficiently compute the MPPI. Formally, let  $G = (\mathcal{V}, \mathcal{F}, \mathcal{E})$  be a factor graph where  $\mathcal{V}$  is the set of variables,  $\mathcal{F}$  is the set of factors, and  $\mathcal{E}$  is the set of edges incident between the sets  $\mathcal{V}$  and  $\mathcal{F}$  (Kschischang et al., 2001). A factor  $f(v, v')$  represents contact between two users such that  $f(v, v')$  is adjacent to  $v, v' \in \mathcal{V}$ . Figure 1 illustrates a simple factor graph. Note that in risk propagation, the aim is to maximize individual MPPIs (Ayday et al., 2021). This contrasts with belief propagation in which the objective is to maximize the full joint distribution (Bishop, 2006).

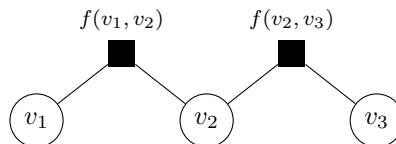


Figure 1: A factor graph of 3 variables and 2 factors.

A *message*  $\mu_{v \rightarrow v'} = \{(r, t), \dots\}$  sent from  $v$  to  $v'$  is a nonempty set of risk scores. We assume that contact with others has a non-decreasing effect on the probability of contracting the disease. Thus, risk propagation is similar to the max-sum algorithm in that each variable maintains the magnitude of the maximum risk score it receives (Bishop, 2006).

While it is possible for users to come in contact on multiple occasions, we will later show that it is only necessary to retain the *most recent* time of contact. In doing so, we reduce the time complexity to compute messages and the space complexity to store the

graph. The only purpose of a factor is to compute and relay messages between variables. Thus, we can modify the topology of the factor graph to only contain *users* such that a user  $u \in \mathcal{U}$  corresponds to the *closed neighborhood* of a variable  $v$ :  $u = v \cap \text{ne}(v)$  where  $\text{ne}(v)$  is the *open neighborhood* of  $v$ ,

$$\text{ne}(v) = \{f(v, v') \mid v, v' \in \mathcal{V}; v \neq v'; (v, f(v, v')) \in \mathcal{E}\}.$$

Users are adjacent if there exists a factor between their associated variables in the original factor graph. Figure 2 depicts this modified topology. Upon receiving a message from a neighbor, a user first assumes the role of its variable to update its value. It then assumes the role of each of its factors to compute and send a message to the respective user. This modification differs from the distributed extension that Ayday et al. (2021) propose in that we do not send duplicate messages to factors. By storing the contact time between users on the edge incident to them, this modified topology is identical to the *contact sequence* representation of a temporal graph or contact network (Holme and Saramäki, 2012),

$$\mathcal{C} = \{(u, u', t) \mid u, u' \in \mathcal{U}; u \neq u'; t \in \mathbb{R}_{\geq 0}\},$$

where a triple  $(u, u', t)$  is called a *contact*. In the context of risk propagation,  $t$  is the starting time at which users  $u, u'$  most recently came in contact. Henceforth, we imply this modification.

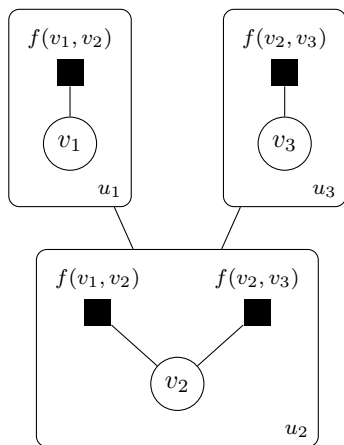


Figure 2: A temporal graph view of Figure 1 that contains 3 user nodes.

It is important to mention that our usage of a temporal graph differs from its typical usage in the field of epidemiology, which focuses on modeling and

analyzing the spreading dynamics of disease (Riolo et al., 2001; Danon et al., 2011; Lokhov et al., 2014; Craft, 2015; Pastor-Satorras et al., 2015; Koher et al., 2019; Zino and Cao, 2021). In contrast, we use a temporal graph to infer the MPPI. As a result, we will introduce a new form of reachability that synthesizes message-passing and the temporal dynamics of the graph in Section 3.4. As noted by Holme and Saramäki (2012), the transmission graph provided by Riolo et al. (2001) “cannot handle edges where one vertex manages to not catch the disease.” Notably, our usage of a temporal graph does allow for such cases by extending the possibility of infection from a binary outcome to a continuous one.

Ayday et al. (2021) define contact as a contiguous duration of 15 minutes in which two individuals are within close proximity. While they claim this is in accordance with the guidance by the Centers for Disease Control and Prevention (CDC), it is important to clarify that the CDC consider these 15 minutes *over a 24-hour time window* (2021). Determining if two individuals satisfy this criterion is challenging from a privacy perspective. Indeed, the ability to link the activity between users over the course of a relatively extended period of time conflicts with approaches that utilize ephemeral identifiers as a means to mitigate privacy risk (Troncoso et al., 2020; Apple Inc. and Google LLC, 2021). We shall remain consistent with Ayday et al. (2021) in our definition of contact, but note that a shorter duration of contiguous contact may also be considered.

We utilize the actor model to achieve scalable performance (Baker and Hewitt, 1977; Agha, 1986). Let  $K \in \mathbb{N}_{>0}$  be the number of actors, where each actor is a subgraph  $G_k \in \mathcal{G}$  of users that is induced by a partitioning algorithm (Buluç et al., 2016) or a clustering algorithm (Aggarwal and Wang, 2010). Formally, we apply a surjective function  $\sigma : \mathcal{U} \rightarrow \mathcal{G}$  that maps each user to exactly one subgraph or actor. Actors communicate with each other via message passing. Typically, inter-actor communication is slower than intra-actor communication, such as when each actor is a separate process. Thus, using a partitioning or clustering algorithm that minimizes communication overhead between actors is key to maximizing the parallelization performance gain. While the partitioning/clustering of the graph is a component of risk propagation, a formal evaluation of different methods is beyond the scope of this work.

We associate with each actor a unique identifier, its *mailing address*, and a buffer, its *remote mailbox*, for

storing messages received from other actors. In practice, each actor also has a separate *local mailbox* that it uses to manage communication between its own users. This local mailbox incurs less overhead than the remote mailbox since the latter typically involves the usage of concurrent primitives (e.g., a lock). To send a message, we must know the mailing address of the receiving actor and the identity of the receiving user. If the mailing address of the sending actor is the same as the receiving actor, then the message is placed in its local mailbox. Otherwise, the message is placed in the remote mailbox of the receiving actor. In addition to maintaining the state of all of the users in its subgraph, an actor also keeps a mapping between mailing addresses and remote mailboxes for all other actors. We do not know *a priori* which actors will need to communicate with each other before partitioning the graph, so we allow an actor the ability to communicate with all other actors.

Briefly, the following is an example, based on Figure 2, of this communication pattern. Suppose  $u_1, u_2 \in G_1$  and  $u_3 \in G_2$  where  $G_1, G_2$  are distinct actors. Then, for  $u_1$  to send a message to  $u_2$ , it must use  $f(v_1, v_2)$  to compute the message and place it in the local mailbox of  $G_1$ . For  $u_2$  to send a message to  $u_3$ , it must use  $f(v_2, v_3)$  to compute the message and place it in the remote mailbox of  $G_2$ .

While we assume  $K \ll |\mathcal{U}|$  for our evaluation of risk propagation, it is possible for  $K = |\mathcal{U}|$  in practice. In this scenario, each user is an actor that communicates with other actors whose user they came into contact. Thus, our formulation of risk propagation that uses asynchronous, parallel message-passing holds for any partitioning of the contact network.

### 3.2. Algorithms

With these preliminary details, we can now introduce the formal algorithms<sup>3</sup>. Algorithm 1 defines the main message-passing procedure. We constrain the set of initial risk scores  $\mathcal{S} = \{(r, t) \mid t_{\text{now}} - t \leq L\}$  to those that were computed within the last  $L = 14$  days, which assumes that a risk score has finite relevance. We constrain the set of contacts  $\mathcal{C}$  similarly. Each actor returns its computed exposure scores when the stopping condition in Algorithm 2.3 is satisfied. Note that the initial risk scores of a user  $u$ , denoted  $\mathcal{S}(u)$ , includes the exposure scores from the last  $L$  days and its most recently computed symptom score.

3. “Algorithm  $x.y$ ” refers to step  $y$  of Algorithm  $x$ .

---

#### Algorithm 1: Risk Propagation, Main

---

1. Create the graph  $G$ : for each  $(u, u', t) \in \mathcal{C}$ , add an edge between  $u, u'$  and store  $t$ .
  2. Partition  $G$  into  $K$  disjoint subgraphs (actors) w.r.t. a partitioning/clustering function  $\sigma(\cdot)$ .
  3. Partition the scores  $\mathcal{S}$  w.r.t.  $\sigma(G)$ .
  4. Send  $\mathcal{S}_k$  to  $G_k$  for  $k \in \mathbb{N}_{[1, K]}$ .
  5. Collect the computed exposure scores from all actors:  $\mathcal{R} \equiv \cup_k \mathcal{R}_k$  (see Algorithm 2).
- 

Algorithm 2 describes the behavior of an actor. In step 1, we define the attributes  $\text{init}(u)$  and  $\text{curr}(u)$  of a user  $u$ . The former is what determines if we should send a computed message in Algorithm 3, and the latter is what we update during message passing. As in Ayday et al. (2021), we assume that risk transmission is incomplete by applying a transmission rate of  $\alpha = 0.8 \in \mathbb{R}_{(0,1)}$  (Hamner et al., 2020). Note that we use  $\alpha$  to denote the transmission rate, instead of  $\tau$  in Ayday et al. (2021). Step 3c follows from belief propagation in that we effectively marginalize over the factor  $f(u, u')$ .

The stopping condition in step 3 is satisfied when at least one of the following criterion hold: (1) *maximum runtime*, the actor has run for a duration of  $D$ ; (2) *early stop*, for all  $u \in G_k$ ,  $\text{curr}(u)$  has not been updated after receiving  $M$  messages; and (3) *timeout*, the actor has not received a message after  $T$  time. If the parameter of a criterion is not set explicitly, we ignore it. In other words, the parameters have default values  $D = M = T = \infty$ . Thus, at least one of the criterion should be configured; otherwise, the actor will never terminate. Note that we cannot use a global iteration count or tolerance as stopping criteria, as used by Ayday et al. (2021), since the message passing is done asynchronously and in-parallel. While such criteria are convenient, they require a synchronization barrier when used in parallel graph processing, which can degrade performance (Han and Daudjee, 2015).

Algorithm 3 describes how we compute and send a message. As indicated by Algorithm 2.2,  $\mu_{u' \rightarrow u}$  in Algorithm 3.1 is initially the risk scores of  $u$ . Thus,  $u = u'$  only when sending the first message to each neighbor. For all subsequent messages,  $u \neq u'$  and

**Algorithm 2:** Risk Propagation, Actor (Main).

1. Upon receiving  $\mathcal{S}_k$ , for each  $u \in G_k$ , let
  - (a)  $\text{init}(u)$  be the initial message; the maximum risk score of  $u$ , scaled by  $\alpha$ ; and
  - (b)  $\text{curr}(u)$  be the current value; initially, the magnitude of the maximum risk score of  $u$ .
2. For each  $u \in G_k$ , compute and send  $\mu_{u \rightarrow v}$  using  $\mathcal{S}(u)$ , for each  $v \in \text{ne}(u)$  (see Algorithm 3).
3. While the stopping condition is unsatisfied,
  - (a) Receive  $\mu_{u' \rightarrow u}$  s.t.  $u \in G_k$  and  $u' \in \text{ne}(u)$ .
  - (b) Update the current value of  $u$ :

$$\text{curr}(u) \leftarrow \max(r_{u' \rightarrow u}, \text{curr}(u)).$$

- (c) For each  $v \in \text{ne}(u) \setminus u'$ , compute and send  $\mu_{u \rightarrow v}$  (see Algorithm 3).
4. Collect exposure scores:

$$\mathcal{R}_k \equiv \{(\text{curr}(u), t_{\text{now}}) \mid u \in G_k\}.$$

$\mu_{u' \rightarrow u}$  is a singleton that contains the risk score sent from  $u'$ . In the context of a singleton message  $\mu_{u' \rightarrow u}$ , we slightly abuse the notation when referring to the magnitude  $r_{u' \rightarrow u}$  and time  $t_{u' \rightarrow u}$  of the contained risk score.

In step 1, we include a time buffer of  $B = 2 \in \mathbb{R}_{\geq 0}$  days to account for the possibility that the onset of infection precludes symptoms. We assume that all risk scores with a time later than the buffered time of contact are irrelevant. Assuming that we run risk propagation at least every  $B$  days, it is not necessary to persist contacts (i.e., edges) that are older than  $B$  days. For a given user  $u$  and neighbor  $u'$ , it is impossible for  $u$  to send  $u'$  a risk score higher in magnitude than what it previously sent if it has been more than  $B$  days after their most recent time of contact. In other words, the MPPI of user  $u'$  will already account for any risk score of user  $u$  after  $B$  days of coming in contact. In this way, we can further improve the efficiency of risk propagation by reducing the number of edges in the temporal graph.

For the remaining risk scores in step 2, we select that which has the highest exponentially-weighted value, where we weight based on the time difference

(in days) between the time of the message and the time of the contact. This assumes that older risk scores have less relevance. In step 3, we use the logarithmic transform, instead of the exponential form, to ensure numerical stability. However, we must ensure that  $r > 0$  when finding the logarithm of each risk score magnitude. For this reason, we use a small number  $\epsilon = 10^{-7} \in \mathbb{R}_{>0}$  in place of  $r$  when  $r < \epsilon$ . While we use an exponential time constant  $\tau = 1 \in \mathbb{R}_{>0}$ , it is possible to modify this to refine the scaling. Specifically, a higher  $\tau$  will further discriminate against older risk scores. Observe that the effect of  $\tau$  is only relevant when initially determining which risk score should be sent to each neighbor since all subsequent message computations only involve one risk score.

Because we allow for a buffer  $B \geq 0$ , it is possible that  $t - t_{uu'} > 0$ . Semantically, we assume that a contact can introduce at most the risk of a user. We therefore cap the weight of a risk score at 0. If multiple risk scores have times such that  $t - t_{uu'} > 0$ , then we select the maximum risk score only on the basis of its magnitude.

The final aspect of Algorithm 3 is to determine if we should send a computed message. Notice that by using the most recent time of contact in step 1, we avoid the need to store and compare multiple times of contact, as suggested by [Ayday et al. \(2021\)](#). This is possible because we only use the time of contact as a filter to determine which risk scores we should consider. That is, given two times of contact  $t_1, t_2$  such that  $t_1 \leq t_2$ , then any risk score with time  $t \leq t_1 + B$  trivially satisfies  $t \leq t_2 + B$ . Therefore, we only require the most recent time of contact.

The following approach differs from [Ayday et al. \(2021\)](#) in that we allow no message to be sent, as opposed to sending a “null” message with a risk score magnitude of 0. By avoiding ineffective messages, we can improve the efficiency of risk propagation. The purpose of sending a message is to possibly update the value of some other user in the graph. Evidently, sending a risk score with a lower magnitude than the current value of the receiving user will not change its value. However, depending on the time of the risk score, the receiving user may still propagate a computed message which subsequently results in an update to some other reachable user in the graph. Notice that the magnitude of a risk score monotonically decreases as it propagates through the graph because we scale its magnitude by  $\alpha$  each time it is sent. Thus, the magnitude of a risk score exponentially decays with a rate constant  $\log(\alpha)$ . Because

of how we filter in step 1, it is possible that a risk score with a lower magnitude than what a user previously sent can change the value of another user if it is sufficiently old.

We can combine both of these aspects into a heuristic that allows us to parametrize the trade-off between completeness and efficiency. Let  $\gamma \in \mathbb{R}_{[0,1]}$  be the *send tolerance* such that we only send a message  $\mu_{u \rightarrow v}$  if  $r_{u \rightarrow v} \geq \gamma \cdot \text{init}(u)$ . In addition to comparing the magnitude, we must also compare the time to the initial message. Assuming a message satisfies the magnitude condition, then a newer message is less likely to be propagated. Hence, it is only useful to send a message if it is at least as old as the initial message. This send condition is expressed in Algorithm 3.5. If  $\gamma > 0$ , this send condition will eventually cause actors to stop passing messages.

---

**Algorithm 3:** Risk Propagation, Actor (Message).

---

1. Consider only the risk scores in the message  $\mu_{u' \rightarrow u}$  that may have been transmitted:

$$\mu'_{u' \rightarrow u} \leftarrow \{(r, t) \mid t \leq t_{uu'} + B\}.$$

2. Compute the time difference (in days) for each remaining risk score:

$$\Delta \leftarrow \{(r, t, \delta) \mid \delta = \min(t - t_{uu'}, 0)\}.$$

3. Compute the maximum weighted message:

$$\mu_{u \rightarrow v} \leftarrow \arg \max_{\mu \in \Delta} \{\log(\max(r, \epsilon)) + \delta/\tau\}.$$

4. Scale by the transmission rate:

$$r_{u \rightarrow v} \leftarrow \alpha \cdot r_{u \rightarrow v}.$$

5. If  $r_{u \rightarrow v} \geq \gamma \cdot \text{init}(u)$  and  $t_{u \rightarrow v} \leq \text{init}(u)$ , send the message  $\mu_{u \rightarrow v}$ .
- 

### 3.3. Complexity

Risk propagation has time complexity  $\mathcal{O}(|\mathcal{C}|)$  because the number of messages that are required is proportional to the number of contacts. This is a tighter bound than Ayday et al. (2021) as they state that the worst-case time complexity is  $\mathcal{O}(s^2)$ , where  $s$  is the number of users. The space complexity of risk

propagation is also  $\mathcal{O}(|\mathcal{C}|)$  because we must store the contacts as well as the attributes and neighborhood of each user. In practice, we use an adjacency list representation of the graph.

### 3.4. Message Reachability

A fundamental concept in reachability analysis on a temporal graph is a *time-respecting path*, which is defined as a contiguous sequence of contacts with non-decreasing time. Thus, node  $u$  is *temporally reachable* (Moody, 2002) from node  $v$  if there exists a time-respecting path from  $v$  to  $u$ . Several quantities derived from the notion of a time-respecting path have been developed to quantify reachability in a temporal graph: the *set of influence of a node  $v$* , or the set of nodes that can be reached by a time-respecting path from node  $v$ ; the *reachability ratio*, or the fraction of node pairs that have a time respecting path between them; and the *source set of a node  $v$* , or the set of nodes that can reach node  $v$  by a time-respecting path (Holme and Saramäki, 2012).

In risk propagation, message passing operates on a looser constraint than requiring temporal reachability. In this way, we can define an estimate of the reachability of an initial risk score for a given user. We call this the *estimated message reachability* of user  $u$  and denote it as  $\hat{m}_\theta(u)$ . The set of parameters  $\theta$  includes the transmission rate  $\alpha$ , the send tolerance  $\gamma$ , and the initial message  $\text{init}(v)$  of some reachable  $v$  from  $u$ . Using the send condition in Algorithm 3.5,

$$\alpha^{\hat{m}_\theta(u)-1} \cdot \text{init}(u) \leq \gamma \cdot \text{init}(v) \quad (1)$$

where the left-hand side is the value of the initial message sent by  $u$  when  $\hat{m}_\theta(u) = 1$ , and the right-hand side is the value required by some reachable  $v$  to propagate the initial message sent by  $u$ . Solving for  $\hat{m}_\theta(u)$  in Equation (1),

$$\hat{m}_\theta(u) \leq 1 + \log_\alpha \left( \gamma \cdot \frac{\text{init}(v)}{\text{init}(u)} \right), \quad (2)$$

where  $\hat{m}_\theta(u) = 0$  if  $\text{init}(u) = 0$  and  $\hat{m}_\theta(u) = \infty$  if  $\gamma \cdot \text{init}(v) = 0$ . Formally, a user  $v$  is *message reachable* from user  $u$  if there exists a path from  $u$  to  $v$  such that all intermediate users satisfy Equation (2) and have a time of contact of at least  $t - B$ , where  $t$  is the time of the risk score.

We can find the *actual message reachability*  $m_\theta(u)$  by applying an augmented shortest-path algorithm (Johnson, 1977) such that we start from user  $u$  and

iteratively send its initial message to reachable users. By doing so, we also account for the temporal component of the send condition in Algorithm 3.5. In this way, message reachability is a similar measure to the set of influence. We can define analogous modifications to the reachability ratio and source set. In practice, because we constrain risk scores to be at most  $L \geq B$  days old, any non-isolated user  $u$  is guaranteed to have message reachability  $m_\theta(u) \geq 1$ .

Message reachability is a measure for estimating the size of the induced subgraph (i.e., set of users) that can be impacted by the risk of a user. From the perspective of efficiency, it indicates that a lower send tolerance will generally result in higher message reachability, at the cost of computing and passing (likely) ineffective messages. Message reachability also allows us to quantify the effect of the transmission rate. Unlike the send tolerance, the transmission rate is intended to be derived from epidemiology in order to characterize the infectivity of the disease. Thus, message reachability allows us to characterize the propagation of risk as a dynamic process on a temporal graph (Barrat and Cattuto, 2013).

## 4. Evaluation

### 4.1. Experimental Design

Unless stated otherwise, we assume the following parameter values: time buffer  $B = 2$  days, transmission rate  $\alpha = 0.8$ , send tolerance  $\gamma = 0.6$ , time constant  $\tau = 1$ , zero approximation  $\epsilon = 10^{-7}$ , timeout  $T = 3$  seconds, maximum duration  $D = 1$  hour, early stop  $M = 10 \cdot (\text{number of users})$ , and random seed 12345. One such exception to these default values is that we use a timeout of  $T = 0$  whenever we use  $K = 1$  actor. For all experiments, we utilized the high-performance computing cluster of Case Western Reserve University. For efficiency experiments, we used 8 CPUs and 16GB RAM. For real-world experiments, we used 4 CPUs and 8GB RAM. For scalability experiments, we used 8–12 CPUs and 16–64GB RAM. All experiments were run on a single cluster node.

Risk propagation requires a partitioning or clustering algorithm, as described in Algorithm 1. We used pymetis<sup>4</sup>, a Python implementation of the METIS partitioning algorithm (Karypis and Kumar, 1998). We configured METIS to use  $k$ -way partitioning with a load imbalance factor of 0.2, to attempt contiguous

partitions that have minimal inter-partition connectivity, to apply 10 iterations of refinement during each stage of the uncoarsening process, and to use the best of 3 cuts. As stated in Section 3, comparing different partitioning methods is beyond the scope of this work. We acknowledge that the quality of the partitioning impacts the performance of risk propagation, and that more scalable approaches than METIS exist (Buluç et al., 2016; Moussawi et al., 2021).

We use NetworkX<sup>5</sup> (Hagberg et al., 2008) to generate synthetic graphs. However, due to its relative memory inefficiency, we convert these graphs into iGraph<sup>6</sup> (Csardi and Nepusz, 2005) objects. For real-world contact networks, we use iGraph directly.

#### 4.1.1. SYNTHETIC GRAPHS

We evaluate the scalability and efficiency of risk propagation on three types of graphs: a random geometric graph [RGG] (Dall and Christensen, 2002), a benchmark graph [LFRG] (Lancichinetti et al., 2008), and a clustered scale-free graph [CSFG] (Holme and Kim, 2002). Together, these graphs demonstrate some aspects of community structure (Fortunato, 2010) which allows us to more accurately measure the performance of risk propagation. When constructing a RGG, we follow a rather arbitrary equation to determine the radius parameter,

$$r(n) = \min\left(1, 0.25^{\log_{10}(n)-1}\right),$$

where  $n$  is the number of users. This allows us to scale the size of the graph while maintaining reasonable density. We use the following parameter values to create LFRGs: mixing parameter  $\mu = 0.1$ , degree power-law exponent  $\gamma = 3$ , community size power-law exponent  $\beta = 2$ , degree bounds  $(k_{\min}, k_{\max}) = (3, 50)$ , and community size bounds  $(s_{\min}, s_{\max}) = (10, 100)$ . Our choices align with the suggestions by Lancichinetti et al. (2008) in that  $\gamma \in \mathbb{R}_{[2,3]}$ ,  $\beta \in \mathbb{R}_{[1,2]}$ ,  $k_{\min} < s_{\min}$ , and  $k_{\max} < s_{\max}$ . To build CSFGs, we add  $m = 2$  edges for each new user and use a triad formulation probability of  $P_t = 0.95$ . For all graphs, we remove self-loops and isolated users.

The following defines our data generation process. Let  $p$  be the probability of a user being “high risk” (i.e., having a risk score magnitude  $r \geq 0.5$ ) Then, with probability  $p = 0.2$ , we sample  $L+1$  values from the uniform distribution  $\mathbb{U}_{[0.5,1]}$ . Otherwise, we sample  $L+1$  values from  $\mathbb{U}_{[0,0.5]}$ . This assumes symptom

4. <https://github.com/inducer/pymetis>

5. <https://networkx.org/>

6. <https://igraph.org/>

scores and exposure scores are computed daily and includes the present day. We generate the times of these risk scores by sampling a time offset  $t_{\text{off}} \sim \mathbb{U}_{[0;86,400]}$  (in seconds) for each user such that

$$\{t_d \mid t_d = t_{\text{now}} + t_{\text{off}} - d \text{ days}; d \in \mathbb{N}_{[0,L]}\}.$$

The edges in the generated graph define the user interactions. To generate a time of contact, we follow the same procedure for risk scores, except that we randomly sample one of the  $L + 1$  times and use that as the time of contact.

We evaluate the effect of varying the transmission rate and send tolerance such that

$$(\gamma, \alpha) \in \{0.1, 0.2, \dots, 1\} \times \{0.1, 0.2, \dots, 0.9\}. \quad (3)$$

For all  $\gamma, \alpha$ , we create a graph with 5,000 users and partition them among  $K = 2$  actors.

To measure the scalability of risk propagation, we consider  $n \in \mathbb{N}_{[10^2, 10^4]}$  users in increments of 100 and collect 10 iterations for each  $n$ . The number of actors we use depends on  $n$  such that

$$K(n) = \begin{cases} 1, & \text{if } n \in [10^2, 10^3) \\ 2, & \text{if } n \in [10^3, 10^4] \end{cases}.$$

We keep  $K$  small because of the number of users we select. Increasing  $K$  for our selection of  $n$  did not result in further performance improvements due to the communication overhead.

#### 4.1.2. REAL-WORLD GRAPHS

We analyze the efficiency of risk propagation on three real-world contact networks (see the ‘‘Data and Code Availability’’ section at the beginning of the paper). Because of limited availability of large-scale contact networks, we do not use real-world contact networks to measure the scalability of risk propagation. We defer to [C’enois and Barrat \(2018\)](#) for detailed discussion and analysis on the contact networks we use. Contacts are detected using radio-frequency identification (RFID) instead of Bluetooth, but the interactions they represent are effectively same. To avoid eliminating a large number of contacts, we only require 20 seconds of proximal interaction to be ‘‘in contact.’’ This definition corresponds to the time interval used by the RFID system to detect interaction between participant sensors. However, we still use the most recent time of interaction to define the contact. We use a single, aggregate graph for each data set. Figure 3 shows the contact graph for each data

set, according to our modified definition of ‘‘contact.’’ We used Gephi<sup>7</sup> ([Bastian et al., 2009](#)) to visualize the graphs.

To ensure that all risk scores are initially propagated, we shift all raw contact times forward by  $t_{\text{now}}$  and use  $(t_{\text{now}} - 1 \text{ day})$  when generating the times of risk scores. In this way, we ensure the most recent risk score is still older than the first contact time. Risk score magnitudes are generated in the same manner as described in Section 4.1.1 with the exception that we only generate one score. Lastly, we perform 10 iterations over each data set with different risk scores to obtain an average performance.

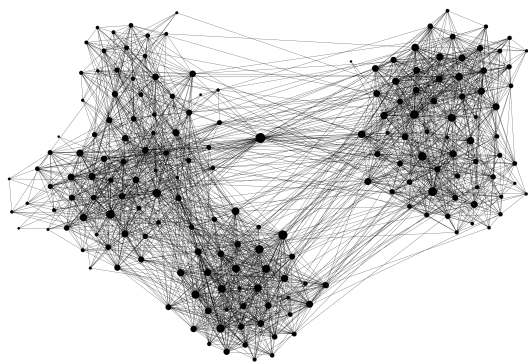
## 4.2. Results

### 4.2.1. EFFICIENCY

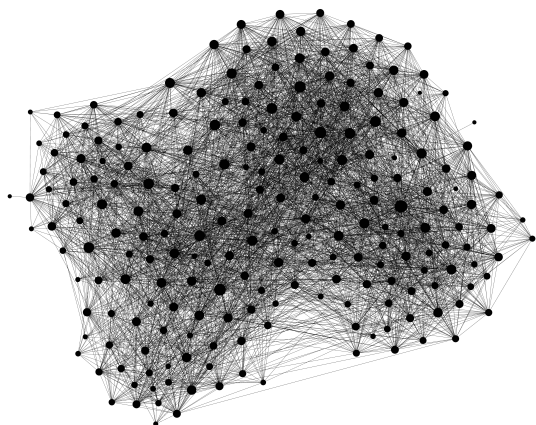
Prior to measuring scalability and real-world performance, we observed the effects of send tolerance and transmission rate on the efficiency of risk propagation. As ground truth, we used the maximum number of updates for a given transmission rate. Figure 4 indicates that a send tolerance of  $\gamma = 0.6$  consistently permits 99% of the possible updates. Beyond  $\gamma = 0.6$ , however, the transmission rate has considerable impact on the number of updates, regardless of the graph. As noted in Section 3.4, send tolerance allows us to quantify the trade-off between completeness and efficiency. Thus, a send tolerance of  $\gamma = 0.6$  optimizes for both criteria.

Unlike the number of updates, Figure 4 shows a more variable relationship with respect to runtime and number of messages. While, in general, transmission rate (send tolerance) has a direct (resp. inverse) relationship with runtime and number of messages, the graph topology seems to have an impact on this fact. Namely, the LFRG displayed relatively less variability across send tolerance and transmission rate than the RGG and CSFG, which is the cause for the large interquartile ranges. For this reason, it is useful to consider the lower quartile  $Q_1$ , the median  $Q_2$ , and the upper quartile  $Q_3$  for ‘‘typical’’ performance. For transmission rate  $\alpha = 0.8$  and send tolerance  $\gamma = 0.6$ , risk propagation demonstrates notable improvement in efficiency with  $(Q_1, Q_2, Q_3) = (0.13, 0.13, 0.46)$  for normalized runtime and  $(Q_1, Q_2, Q_3) = (0.13, 0.15, 0.44)$  for normalized number of messages.

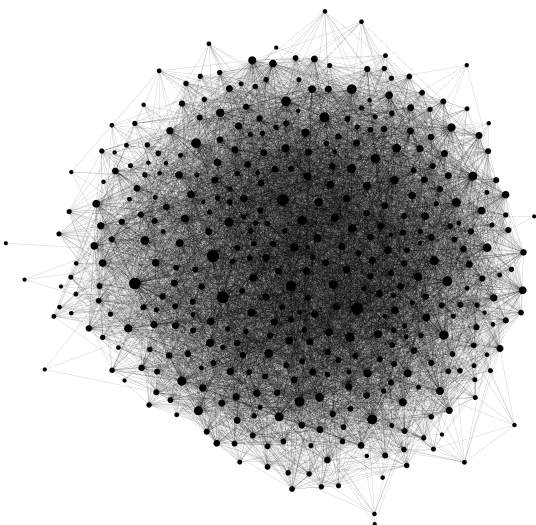
7. <https://gephi.org/>



(a) Thiers13 (180 users; 2,220 contacts)



(b) InVS15 (217 users; 4,274 contacts)



(c) SFHH (403 users; 9,565 contacts)

Figure 3: SocioPatterns contact graphs.

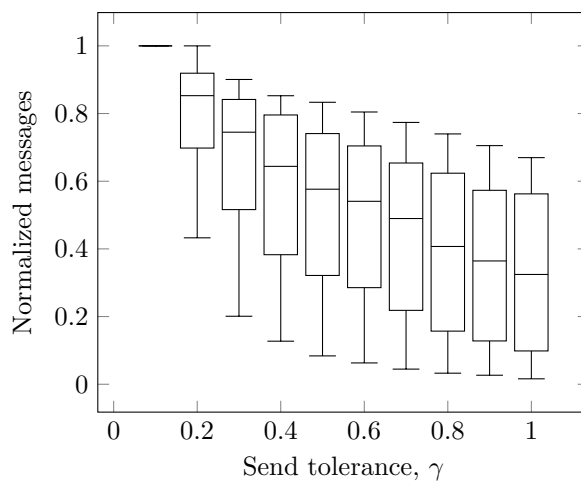
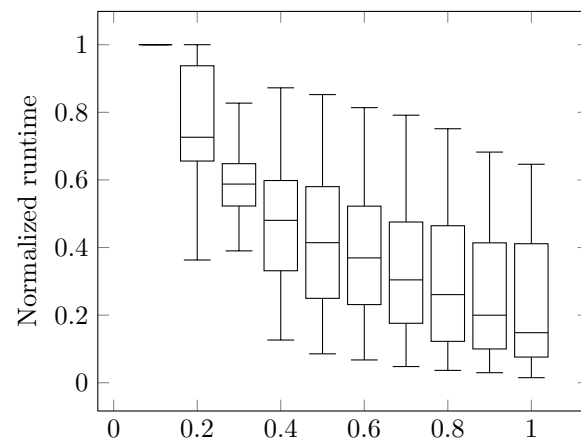
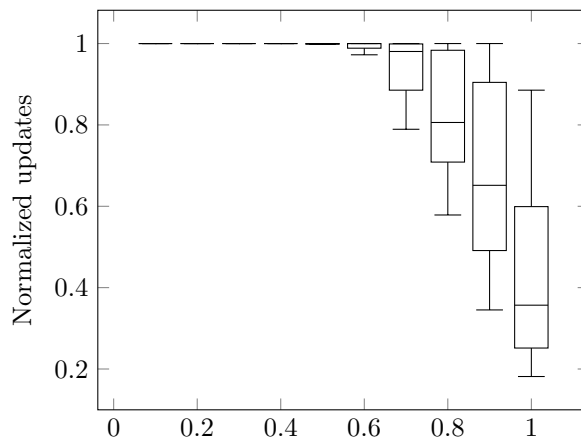


Figure 4: The effects of send tolerance and transmission rate on efficiency. All dependent variables are normalized across graphs and transmission rates.

#### 4.2.2. MESSAGE REACHABILITY

To validate the accuracy of message reachability (see Section 3.4), we collected estimated and actual message reachability data for real-world and synthetic graphs. For the latter set of graphs, we observed reachability while sweeping across the send tolerance and transmission rate, as described in Equation (3).

To compare the relative accuracy of message reachability, let  $m_\theta/\hat{m}_\theta$  be the *actual/estimated message reachability ratio* (A/E MRR). Overall, Equation (2) is a good estimator of actual message reachability. Across all synthetic graphs, Equation (2) modestly underestimated  $m_\theta$  with quartiles  $(Q_1, Q_2, Q_3) = (0.71, 0.84, 0.98)$  for the A/E MRR. For a transmission rate  $\alpha = 0.8$  and send tolerance  $\gamma = 0.6$ , the A/E MRR exhibited quartiles  $(Q_1, Q_2, Q_3) = (0.52, 0.77, 1.12)$  and  $(Q_1, Q_2, Q_3) = (0.79, 0.84, 0.93)$ , respectively. Table 1 provides the mean A/E MRR for both synthetic and real-world graphs. Figure 5 indicates that moderate values of send tolerance tend to result in a more stable A/E MRR, with lower (higher) send tolerances underestimating (resp. overestimating)  $m_\theta$ . With regard to transmission rate,  $m_\theta/\hat{m}_\theta$  tends to decrease with increasing  $\alpha$ , but also exhibits larger interquartile ranges.

Because Equation (2) does not account for contact temporality, it is not a perfect estimator of  $m_\theta$ . With lower send tolerances and higher transmission rates, Equation (2) suggests higher message reachability. However, because a message is only passed under certain conditions (see Algorithm 3), this causes Equation (2) to overestimate  $m_\theta$ . While Equation (2) is a theoretical upper bound on  $m_\theta$ , it is possible for Equation (2) to overestimate  $m_\theta(u)$  if the specified value of  $\text{init}(v)$  overestimates the true magnitude of the initial message sent by a reachable  $v$  of  $u$ . When computing  $m_\theta/\hat{m}_\theta$  for Figure 5, we used the mean initial message across all users for  $\text{init}(v)$ , so  $m_\theta/\hat{m}_\theta > 1$  in some cases.

#### 4.2.3. SCALABILITY

Figure 6 describes the runtime behavior of risk propagation on synthetic graphs. The peculiar runtime of CSFGs may have been partially caused by the randomness of the METIS algorithm but requires further investigation. A linear regression fit explains ( $R^2 = 0.52$ ) the runtime of LFRGs and RGGs with a slope  $m = (1.1 \pm 0.1) \cdot 10^{-3}$  seconds per contact and intercept  $b = 4.3 \pm 1.6$  seconds ( $\pm 1.96 \cdot \text{SE}$ ).

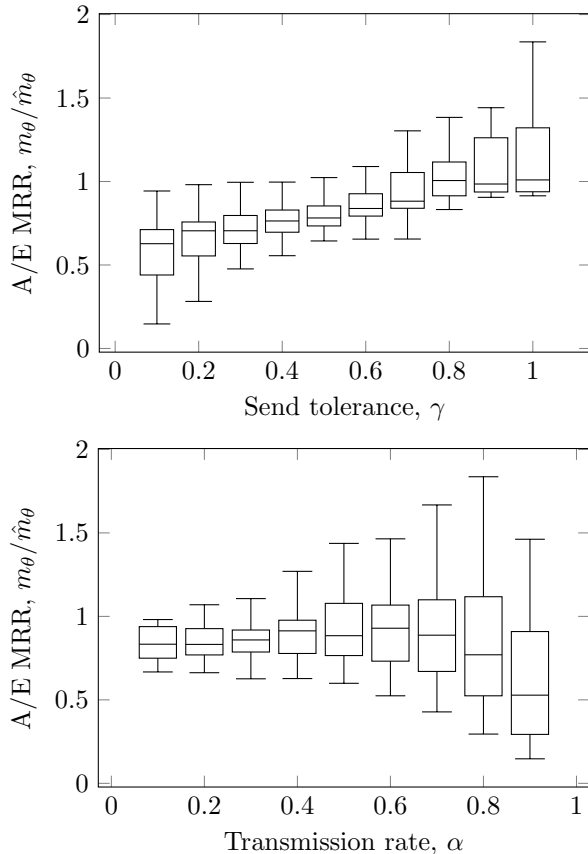


Figure 5: The effects of send tolerance and transmission rate on the A/E MRR. Independent variables are grouped across graphs.

Table 1: A/E MRR for synthetic and real-world graphs ( $\alpha = 0.8$ ,  $\gamma = 0.6$ ). Synthetic ratios are averaged across parameter combinations. Real-world ratios are averaged across runs.

Setting	$m_\theta/\hat{m}_\theta \pm 1.96 \cdot \text{SE}$
<i>Synthetic</i>	
LFR	$0.88 \pm 0.14$
RGG	$0.74 \pm 0.12$
CSFG	$0.90 \pm 0.14$
	<b><math>0.85 \pm 0.08</math></b>
<i>Real-world</i>	
Thiers13	$0.58 \pm 0.01$
InVS15	$0.63 \pm 0.01$
SFHH	$0.60 \pm 0.01$
	<b><math>0.60 \pm 0.01</math></b>

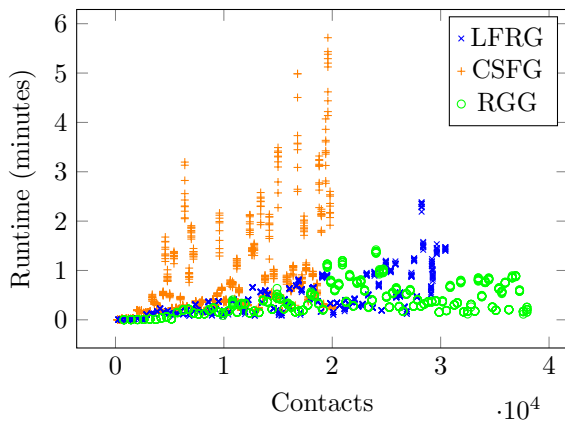


Figure 6: Runtime of risk propagation on synthetic graphs containing 100–10,000 users and  $\sim 200$ –38,000 contacts.

## 5. Conclusions

Applications like ShareTrace are fundamentally collaborative in that users exchange data amongst each other to achieve an objective or gain personal utility. Maintaining personal data ownership and privacy in this collaborative setting while ensuring architectural scalability and security is an ongoing challenge in the fields of machine learning and cloud computing (Cano et al., 2015; Hsieh et al., 2017; Jonas et al., 2017; Singhvi et al., 2017). Our formulation of risk propagation offers better scalability and efficiency than Ayday et al. (2021). It is thus a viable candidate for real-world usage to both track and prevent the spread of infectious diseases. Moreover, message reachability provides researchers and system designers the ability to quantify both the risk of an individual and the effects parameter values have on the efficiency and accuracy of risk propagation.

In future work, we intend to consider mechanisms of establishing decentralized, verifiable communication channels (Abramson et al., 2020) as a means to satisfy the collaborative requirements of user-centric applications, such as ShareTrace. Moreover, we shall consider how privacy-preserving mechanisms, such as differential privacy (Dwork and Roth, 2014), may be utilized in such a setting to minimize the personal risks of widespread data sharing.

## Institutional Review Board (IRB)

This research did not require IRB approval.

## Acknowledgments

Research reported in this publication was partly supported by the Cisco Research University Funding grant number 2800379. This work made use of the High Performance Computing Resource in the Core Facility for Advanced Research Computing at Case Western Reserve University.

## References

- Will Abramson, Adam James Hall, Pavlos Papadopoulos, Nikolaos Pitropakis, and William J. Buchanan. A distributed trust framework for privacy-preserving machine learning. In Stefanos Gritzalis, Edgar R. Weippl, Gabriele Kotsis, A. Min Tjoa, and Ismail Khalil, editors, *TrustBus 2020: Trust, Privacy and Security in Digital Business*, volume 12395 of *Lecture Notes in Computer Science*, 2020. doi:[10.1007/978-3-030-58986-8-14](https://doi.org/10.1007/978-3-030-58986-8-14).
- Charu C. Aggarwal and Haixun Wang. A survey of clustering algorithms for graph data. In Ahmed K. Elmagarmid and Amit P. Sheth, editors, *Managing and Mining Graph Data*, volume 40 of *Advances in Database Systems*. Springer, 2010. doi:[10.1007/978-1-4419-6045-0-9](https://doi.org/10.1007/978-1-4419-6045-0-9).
- Gul Abdunabi Agha. *Actors: A Model of Concurrent Computation in Distributed Systems*. MIT Press, 1986. doi:[10.7551/mitpress/1086.001.0001](https://doi.org/10.7551/mitpress/1086.001.0001).
- Nadeem Ahmed, Regio A. Michelin, Wanli Xue, Sushmita Ruj, Robert Malaney, Salil S. Kanhere, Aruna Seneviratne, Wen Hu, Helge Janicke, and Sanjay Jha. A survey of COVID-19 contact tracing apps. *IEEE Access*, 8, 2020. doi:[10.1109/access.2020.3010226](https://doi.org/10.1109/access.2020.3010226).
- Apple Inc. and Google LLC. Privacy-preserving contact tracing, 2021. URL <https://covid19.apple.com/contacttracing>.
- Erman Ayday, Youngjin Yoo, and Anisa Halimi. ShareTrace: An iterative message passing algorithm for efficient and effective disease risk assessment on an interaction graph. In *Proceedings of the 12th ACM Conference on Bioinformatics, Computational Biology, and Health Informatics*, BCB '21, 2021. doi:[10.1145/3459930.3469553](https://doi.org/10.1145/3459930.3469553).
- Henry Baker and Carl Hewitt. Laws for communicating parallel processes. Technical report, Mas-

- sachusetts Institute of Technology, 1977. URL <http://hdl.handle.net/1721.1/41962>.
- Alain Barrat and Ciro Cattuto. Temporal networks of face-to-face human interactions. In Petter Holme and Jari Saramäki, editors, *Temporal Networks, Understanding Complex Systems*. Springer, 2013. doi:[10.1007/978-3-642-36461-7\\_10](https://doi.org/10.1007/978-3-642-36461-7_10).
- Mathieu Bastian, Sebastien Heymann, and Mathieu Jacomy. Gephi: An open source software for exploring and manipulating networks. In *Proceedings of the International AAAI Conference on Web and Social Media*, volume 3, 2009.
- Christopher M. Bishop. Pattern recognition and machine learning. In M. I. Jordan, Robert Nowak, and Bernhard Schoelkopf, editors, *Information Science and Statistics*. Springer, 2006.
- Aydin Buluç, Henning Meyerhenke, Ilya Safro, Peter Sanders, and Christian Schulz. Recent advances in graph partitioning. In Lasse Kliemann and Peter Sanders, editors, *Algorithm Engineering: Selected Results and Surveys*. Springer, 2016. doi:[10.1007/978-3-319-49487-6\\_4](https://doi.org/10.1007/978-3-319-49487-6_4).
- Ignacio Cano, Dhruv Mahajan, Giovanni Matteo Fumarola, Arvind Krishnamurthy, Markus Weimer, and Carlo Curino. Towards geo-distributed machine learning. *IEEE Data(base) Engineering Bulletin*, 40, 2015. URL <https://www.microsoft.com/en-us/research/publication/towards-geo-distributed-machine-learning/>.
- Centers for Disease Control and Prevention. Quarantine and isolation, 2021. URL <https://www.cdc.gov/coronavirus/2019-ncov/your-health/quarantine-isolation.html>.
- Hyunghoon Cho, Daphne Ippolito, and Yun William Yu. Contact tracing mobile apps for COVID-19: Privacy considerations and related trade-offs. 2020. doi:[10.48550/arXiv.2003.11511](https://doi.org/10.48550/arXiv.2003.11511).
- Meggan E. Craft. Infectious disease transmission and contact networks in wildlife and livestock. *Philosophical Transactions of the Royal Society B: Biological Sciences*, 370, 2015. doi:[10.1098/rstb.2014.0107](https://doi.org/10.1098/rstb.2014.0107).
- Gabor Csardi and Tamas Nepusz. The igraph software package for complex network research. *InterJournal*, 1695, 2005.
- Jesper Dall and Michael Christensen. Random geometric graphs. *Physical Review E*, 66, 2002. doi:[10.1103/PhysRevE.66.016121](https://doi.org/10.1103/PhysRevE.66.016121).
- Leon Danon, Ashley P. Ford, Thomas House, Chris P. Jewell, Gareth O. Roberts, Joshua V. Ross, and Matthew C. Vernon. Networks and the epidemiology of infectious disease. *Interdisciplinary Perspectives on Infectious Diseases*, 2011, 2011. doi:[10.1155/2011/284909](https://doi.org/10.1155/2011/284909).
- Aaqib Bashir Dar, Auqib Hamid Lone, Saniya Zahoor, Afshan Amin Khan, and Roohie Naaz. Applicability of mobile contact tracing in fighting pandemic (COVID-19): Issues, challenges and solutions. *Computer Science Review*, 38, 2020. doi:[10.1016/j.cosrev.2020.100307](https://doi.org/10.1016/j.cosrev.2020.100307).
- Cynthia Dwork and Aaron Roth. The algorithmic foundations of differential privacy. *Foundations and Trends in Theoretical Computer Science*, 9, 2014. doi:[10.1561/04000000042](https://doi.org/10.1561/04000000042).
- Santo Fortunato. Community detection in graphs. *Physics Reports*, 486, 2010. doi:[10.1016/j.physrep.2009.11.002](https://doi.org/10.1016/j.physrep.2009.11.002).
- Julie Fournet and Alain Barrat. Contact patterns among high school students. *PLoS ONE*, 9, 2014. doi:[10.1371/journal.pone.0107878](https://doi.org/10.1371/journal.pone.0107878).
- Mathieu G'enois and Alain Barrat. Can co-location be used as a proxy for face-to-face contacts? *EPJ Data Science*, 7, 2018. doi:[10.1140/epjds/S13688-018-0140-1](https://doi.org/10.1140/epjds/S13688-018-0140-1).
- Aric A. Hagberg, Daniel A. Schult, and Pieter J. Swart. Exploring network structure, dynamics, and function using NetworkX. In Gaël Varoquaux, Travis Vaught, and Jarrod Millman, editors, *Proceedings of the 7th Python in Science Conference*, 2008.
- Lea Hamner, Polly Dubbel, Ian Capron, Andy Ross, Amber Jordan, Jaxon Lee, Joanne Lynn, Amelia Ball, Simranjit Narwal, Sam Russell, Dale Patrick, and Howard Leibrand. High SARS-CoV-2 attack rate following exposure at a choir practice – Skagit County, Washington, March 2020. *Morbidity and Mortality Weekly Report*, 69, 2020. doi:[10.15585/mmwr.mm6919e6](https://doi.org/10.15585/mmwr.mm6919e6).
- Minyang Han and Khuzaima Daudjee. Giraph unchained: Barrierless asynchronous parallel execution in pregel-like graph processing systems.

- Proceedings of the VLDB Endowment*, 8, 2015. doi:[10.14778/2777598.2777604](https://doi.org/10.14778/2777598.2777604).
- Petter Holme. Modern temporal network theory: a colloquium. *The European Physical Journal B*, 88, 2015. doi:[10.1140/epjb/e2015-60657-4](https://doi.org/10.1140/epjb/e2015-60657-4).
- Petter Holme and Beom Jun Kim. Growing scale-free networks with tunable clustering. *Physical Review E*, 65, 2002. doi:[10.1103/PhysRevE.65.026107](https://doi.org/10.1103/PhysRevE.65.026107).
- Petter Holme and Jari Saramäki. Temporal networks. *Physics Reports*, 519, 2012. doi:[10.1016/j.physrep.2012.03.001](https://doi.org/10.1016/j.physrep.2012.03.001).
- Kevin Hsieh, Aaron Harlap, Nandita Vijaykumar, Dimitris Konomis, Gregory R. Ganger, Phillip B. Gibbons, and Onur Mutlu. Gaia: Geo-distributed machine learning approaching LAN speeds. In *14th USENIX Symposium on Networked Systems Design and Implementation (NSDI 17)*, 2017.
- Donald B. Johnson. Efficient algorithms for shortest paths in sparse networks. *Journal of the ACM*, 24, 1977. doi:[10.1145/321992.321993](https://doi.org/10.1145/321992.321993).
- Eric Jonas, Qifan Pu, Shivaram Venkataraman, Ion Stoica, and Benjamin Recht. Occupy the cloud: Distributed computing for the 99%. In *Proceedings of the 2017 Symposium on Cloud Computing, SoCC '17*, 2017. doi:[10.1145/3127479.3128601](https://doi.org/10.1145/3127479.3128601).
- Brian Karrer and M. E. J. Newman. Message passing approach for general epidemic models. *Physical Review E*, 82, 2010. doi:[10.1103/PhysRevE.82.016101](https://doi.org/10.1103/PhysRevE.82.016101).
- George Karypis and Vipin Kumar. A fast and high quality multilevel scheme for partitioning irregular graphs. *SIAM Journal on Scientific Computing*, 20, 1998. doi:[10.1137/S1064827595287997](https://doi.org/10.1137/S1064827595287997).
- Andreas Koher, Hartmut H. K. Lentz, James P. Gleeson, and Philipp Hövel. Contact-based model for epidemic spreading on temporal networks. *Physical Review X*, 9, 2019. doi:[10.1103/PhysRevX.9.031017](https://doi.org/10.1103/PhysRevX.9.031017).
- Frank R. Kschischang, Brendan J. Frey, and Hans A. Loeliger. Factor graphs and the sum-product algorithm. *IEEE Transactions on Information Theory*, 47, 2001. doi:[10.1109/18.910572](https://doi.org/10.1109/18.910572).
- Christiane Kuhn, Martin Beck, and Thorsten Strufe. Covid notions: Towards formal definitions – and documented understanding – of privacy goals and claimed protection in proximity-tracing services. *Online Social Networks and Media*, 22, 2021. doi:[10.1016/j.osnem.2021.100125](https://doi.org/10.1016/j.osnem.2021.100125).
- Andrea Lancichinetti, Santo Fortunato, and Filippo Radicchi. Benchmark graphs for testing community detection algorithms. *Physical Review E*, 78, 2008. doi:[10.1103/PhysRevE.78.046110](https://doi.org/10.1103/PhysRevE.78.046110).
- Bo Li and David Saad. Impact of presymptomatic transmission on epidemic spreading in contact networks: A dynamic message-passing analysis. *Physical Review E*, 103, 2021. doi:[10.1103/PhysRevE.103.052303](https://doi.org/10.1103/PhysRevE.103.052303).
- Andrey Y. Lokhov, Marc Mézard, Hiroki Ohta, and Lenka Zdeborová. Inferring the origin of an epidemic with a dynamic message-passing algorithm. *Physical Review E*, 90, 2014. doi:[10.1103/PhysRevE.90.012801](https://doi.org/10.1103/PhysRevE.90.012801).
- Federica Lucivero, Nina Hallowell, Stephanie Johnson, Barbara Prainsack, Gabrielle Samuel, and Tamar Sharon. COVID-19 and contact tracing apps: Ethical challenges for a social experiment on a global scale. *Journal of Bioethical Inquiry*, 17, 2020. doi:[10.1007/s11673-020-10016-9](https://doi.org/10.1007/s11673-020-10016-9).
- Tania Martin, Georgios Karopoulos, José Hernández-Ramos, Georgios Kambourakis, and Igor Nai Fovino. Demystifying COVID-19 digital contact tracing: A survey on frameworks and mobile apps. *Wireless Communications and Mobile Computing*, 2020, 2020. doi:[10.1155/2020/8851429](https://doi.org/10.1155/2020/8851429).
- Robert McCune, Tim Weninger, and Greg Madey. Thinking like a vertex: A survey of vertex-centric frameworks for large-scale distributed graph processing. *ACM Computing Surveys*, 48, 2015. doi:[10.1145/2818185](https://doi.org/10.1145/2818185).
- Cristina Menni, Ana M Valdes, Maxim B Freidin, Carole H Sudre, Long H Nguyen, David A Drew, Sajjasurya Ganesh, Thomas Varsavsky, M Jorge Cardoso, Julia S El-Sayed Moustafa, Alessia Visconti, Pirro Hysi, Ruth C E Bowyer, Massimo Mangino, Mario Falchi, Jonathan Wolf, Sebastien Ourselin, Andrew T Chan, Claire J Steves, and Tim D Spector. Real-time tracking of self-reported symptoms to predict potential COVID-19. *Nature Medicine*, 26, 2020. doi:[10.1038/s41591-020-0916-2](https://doi.org/10.1038/s41591-020-0916-2).

- James Moody. The importance of relationship timing for diffusion. *Social Forces*, 81, 2002. URL <http://www.jstor.org/stable/3086526>.
- Adnan El Moussawi, Nacéra Bennacer Seghouani, and Francesca Bugiotti. BGRAP: Balanced GRAPh partitioning algorithm for large graphs. *Journal of Data Intelligence*, 2, 2021. doi:[10.26421/jdi2.2-2](https://doi.org/10.26421/jdi2.2-2).
- Romualdo Pastor-Satorras, Claudio Castellano, Piet Van Mieghem, and Alessandro Vespignani. Epidemic processes in complex networks. *Reviews of Modern Physics*, 87, 2015. doi:[10.1103/RevModPhys.87.925](https://doi.org/10.1103/RevModPhys.87.925).
- Ramesh Raskar, Isabel Schunemann, Rachel Barbar, Kristen Vilcans, Jim Gray, Praneeth Vepakomma, Suraj Kapa, Andrea Nuzzo, Rajiv Gupta, Alex Berke, Dazza Greenwood, Christian Keegan, Shriank Kanaparti, Robson Beaudry, David Stansbury, Beatriz Botero Arcila, Rishank Kanaparti, Vitor Pamplona, Francesco M Benedetti, Alina Clough, Riddhiman Das, Kaushal Jain, Khahlil Louisy, Greg Nadeau, Vitor Pamplona, Steve Penrod, Yasaman Rajae, Abhishek Singh, Greg Storm, and John Werner. Apps gone rogue: Maintaining personal privacy in an epidemic. 2020. doi:[10.48550/arXiv.2003.08567](https://doi.org/10.48550/arXiv.2003.08567).
- Christopher S. Riolo, James S. Koopman, and Stephen E. Chick. Methods and measures for the description of epidemiologic contact networks. *Journal of Urban Health*, 78, 2001. doi:[10.1093/jurban/78.3.446](https://doi.org/10.1093/jurban/78.3.446).
- Arjun Singhvi, Sujata Banerjee, Yotam Harchol, Aditya Akella, Mark Peek, and Pontus Rydin. Granular computing and network intensive applications: Friends or foes? In *Proceedings of the 16th ACM Workshop on Hot Topics in Networks*, HotNets-XVI, 2017. doi:[10.1145/3152434.3152450](https://doi.org/10.1145/3152434.3152450).
- Carmela Troncoso, Mathias Payer, Jean-Pierre Hubaux, Marcel Salathé, James Larus, Edouard Bugnion, Wouter Lueks, Theresa Stadler, Apostolos Pyrgelis, Daniele Antonioli, Ludovic Barman, Sylvain Chatel, Kenneth Paterson, Srdjan Čapkun, David Basin, Jan Beutel, Dennis Jackson, Marc Roeschlin, Patrick Leu, Bart Preneel, Nigel Smart, Aysajan Abidin, Seda Gürses, Michael Veale, Cas Cremers, Michael Backes, Nils Ole Tippenhauer, Reuben Binns, Ciro Cattuto, Alain Barrat, Dario Fiore, Manuel Barbosa, Rui Oliveira, and José Pereira. Decentralized privacy-preserving proximity tracing. 2020. doi:[10.48550/arXiv.2005.12273](https://doi.org/10.48550/arXiv.2005.12273).
- Haohuang Wen, Qingchuan Zhao, Zhiqiang Lin, Dong Xuan, and Ness Shroff. A study of the privacy of COVID-19 contact tracing apps. In Noseong Park, Kun Sun, Sara Foresti, Kevin Butler, and Nitesh Saxena, editors, *Security and Privacy in Communication Networks*, volume 335 of *Lecture Notes of the Institute for Computer Sciences, Social Informatics and Telecommunications Engineering*. Springer International Publishing, 2020. doi:[10.1007/978-3-030-63086-7\\_17](https://doi.org/10.1007/978-3-030-63086-7_17).
- Lorenzo Zino and Ming Cao. Analysis, prediction, and control of epidemics: A survey from scalar to dynamic network models. *IEEE Circuits and Systems Magazine*, 21, 2021. doi:[10.1109/mcas.2021.3118100](https://doi.org/10.1109/mcas.2021.3118100).

## Appendix A. Message Reachability

Given the multivariate nature of message reachability, it is helpful to visualize how it behaves under conditions of various parameter value combinations. Figure 7 includes several line plots of estimated message reachability  $\hat{m}_\theta(u)$  with respect to the initial risk score magnitude of a user  $u$ . For all parameters that are not varying in a given plot, we fix them to either 0.2 or 0.8.

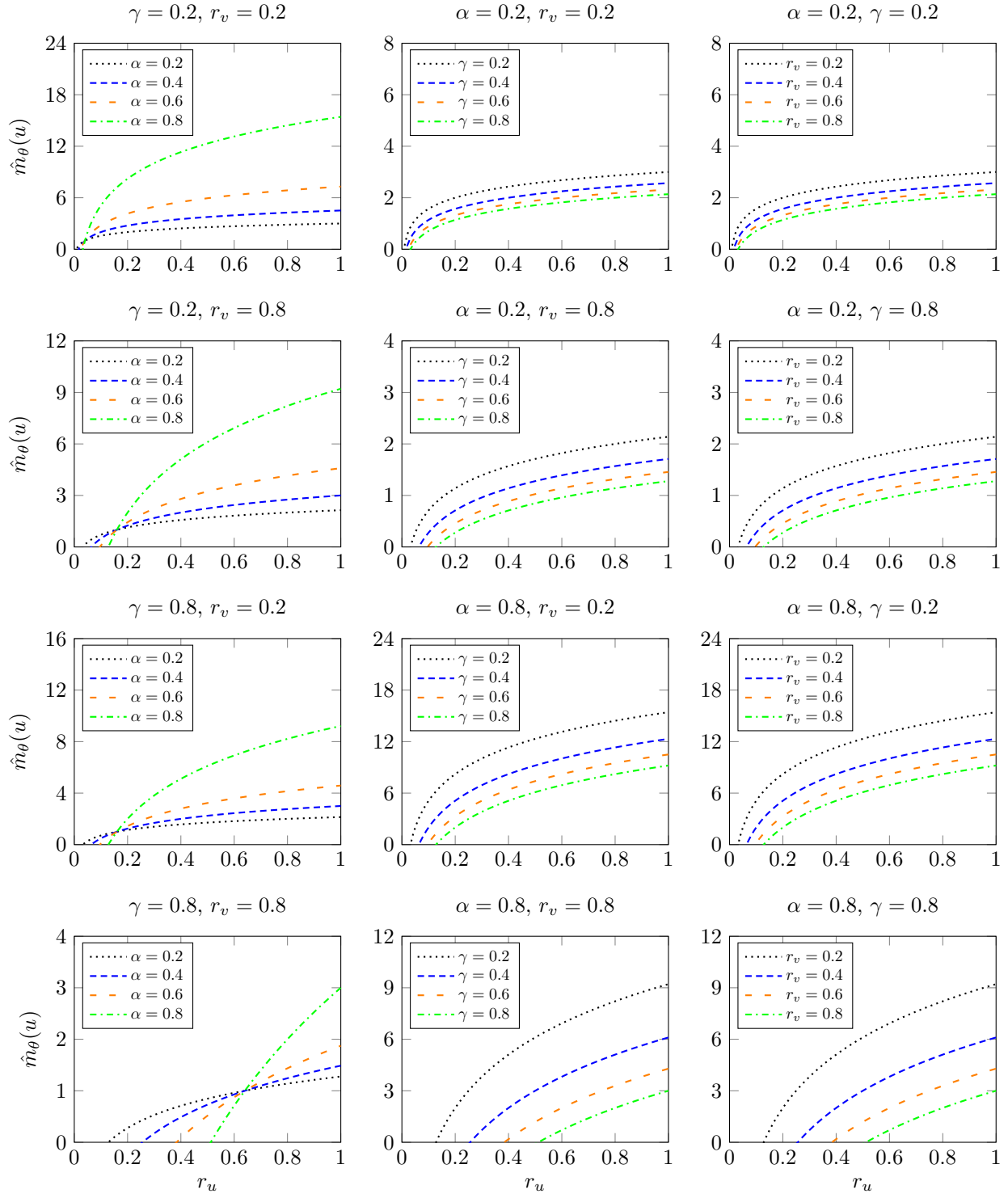


Figure 7: Estimated message reachability  $\hat{m}_\theta(u)$  for different values of the transmission rate  $\alpha$ , the send tolerance  $\gamma$ , and the initial magnitude  $r_v = \text{init}(v)/\alpha$  of the destination user  $v$  with respect to the initial magnitude  $r_u = \text{init}(u)/\alpha$  of the source user  $u$ .